A review of pressure manipulating structure and performance in thermoelectrics

IOP Publishing Journal Title
Journal **XX** (XXXX) XXXXXX https://doi.org/XXXX/XXXX

A review of pressure manipulating structure and performance in thermoelectrics

He Zhang[1,†], Cunyin Zhang[1,†], Duncan H. Gregory[3], Zhanxiang Yin[1], Yaqiang Wang[1], Pan He[1,2,*] and Xin Guo[1,2,*]

[1] School of Materials Science and Engineering, Changchun University of Science and Technology, Changchun 130022, China
[2] Engineering Research Center of Optoelectronic Functional Materials for Ministry of Education, Changchun University of Science and Technology, Changchun 130022, China.
[3] WestCHEM, School of Chemistry, University of Glasgow, Glasgow G12 8QQ, U.K.

E-mail: xguo@cust.edu.cn (X.G.), hepan@cust.edu.cn (P.H.)

Received xxxxxx
Accepted for publication xxxxxx
Published xxxxxx

Abstract

Pressure is a fundamental thermodynamic variable that can create exotic materials and modulate transport properties, motivating prosperous progress in multiple fields. As for inorganic thermoelectric materials, pressure is an indispensable condition during a preparation process, which is employed to compress raw powders into the specific shape of solid-state materials for performing properties characterization. In addition to this function, the extra influence of pressure on thermoelectric performance is frequently underestimated and even overlooked. In this review, we summarize recent progress and achievements of pressure-induced structure and performance in thermoelectrics, emphatically involving the modulation of pressure on crystal structure, electrical transport properties, microstructure, and thermal conductivity. According to various studies, the modulated mechanism of pressure on these items above has been discussed in detail, and the perspectives and strategies have been proposed with respect to applying pressure to improve thermoelectric performance. Overall, the purpose of the review is supposed to enrich the understanding of the mechanisms in pressure-induced transport properties and provide a guidance to rationally design a structural pattern to improve thermoelectric performance.

Keywords: pressure, thermoelectric, crystal structure, microstructure, transport properties

1. Introduction

Energy is a powerful driving force to the development of human civilization. Classical fossil energy as a major resource has been exploited excessively for a long time, subsequently leading to a negative reaction such as seriously environmental pollution and energy crisis. Alternative energy sources are urgently demanded to be explored in order to modify the stress

† These authors contributed equally to this work.

* Author to whom any correspondence should be addressed.

of fossil energy in the sustainable development of society. In this context, thermoelectric technology symbolizes a solid-state energy conversion model, which is capable of directly converting heat into electricity and *vice versa* and has attracted extensive attention in sustainable energy fields [1-5]. The thermoelectric devices, which consists of thermoelectric materials, perform significant advantages such as eco-friendly, reliable performance, long-service period, *etc* [6-8]. However, a low conversion efficiency remains a giant challenge against thermoelectric devices stepping into commercial markets [9]. For this reason, sustained efforts are devoted to improving thermoelectric performance of materials and rationally designing thermoelectric devices in order to boost the widespread application in thermoelectrics [10]. Compared to the design of thermoelectric devices, a high conversion efficiency is extremely dependent upon an improvement in thermoelectric performance, which plays a vital role for the devices. Therefore, the enhancement in performance of existing thermoelectric materials and the exploration of potentially high-performance thermoelectric materials remain dominant subjects in thermoelectrics.

To estimate the thermoelectric performance, a dimensionless figure of merit, zT, is defined as the formula of $zT = S^2\sigma T/\kappa$, where S is the Seebeck coefficient, σ is the electrical conductivity, T is the Kelvin temperature, and κ is the total thermal conductivity consisting of electronic (κ_{ele}) and lattice (κ_{lat}) contributions [11, 12]. The $S^2\sigma$ represents the electrical transport properties, is called as the power factor (PF), and is recognized as a crucial indicator capable of applying to the power generation. A superior zT value is achieved required to a distinguished electrical transport properties coexistent with an inferior total thermal conductivity. However, S, σ, κ_{ele}, and κ_{lat} are interdependent due to the electron-phonon coupling, leading to an extreme difficulty in the improvement of thermoelectric performance [13]. Alternative strategies, such as band engineering [14, 15], phonon anharmonicity [16-18], multiscale defects [19, 20], *etc*., have been confirmed that could properly decouple the electron-phonon transport improving thermoelectric performance in the materials over the last decade. These strategies are generally achieved by optimizing composition and temperature in the matrix, whose essences are identified as the influence of structural modification on thermoelectric transport properties [21]. It is evident that the physical and chemical properties of materials are strongly dependent on the crystal structure [22]. Pressure, as a fundamental thermodynamic variable, can directly modify crystal structure influencing atomic sites, interatomic electrostatic interactions, electronic orbitals, and chemical bonding [23-26], even in the case when the stoichiometry and temperature remain unchanged [27], which implies that thermoelectric transport parameters could be manipulated through applying pressure. Unfortunately, pressure is frequently underestimated and even overlooked in the preparation and performance of materials, despite *in-situ* high-pressure technology has exhibited fantastic effects on microscopic structure and transport properties in various thermoelectric materials (Table 1) [28-36]. We could make pressure incorporate into other thermodynamic variables, if pressure is considered as a conventional variable. This will build a brand-new three-dimensional (3D) space, as shown in Figure 1, consequently extending the investigation and exploration of thermoelectric materials. For the 3D space compared to the conventional modulation (*i.e.* composition and temperature), it might get an opportunity to truly mitigate the electron-phonon coupling and extremely boost thermoelectric performance. In addition to the improvement in thermoelectric properties of existing materials, pressure can create exotic materials *via* introducing structural phase transitions as well [37], which offer a platform for exploring potentially high-performance thermoelectric materials [38-41].

In this review, we summarize recent progress and achievements of pressure-induced structure and performance in thermoelectrics, and elaborate intrinsic mechanisms with respect to the modulation of pressure on thermoelectric transport properties. Based on the conceptions, the major contents would emphatically discuss four subjects as follows: First, the crystal structure influenced by pressure is elaborated in section 2. Meanwhile, it is clarified further that the phase transition caused by pressure contributes to thermoelectric properties. Secondly, we conclude the influence of pressure on the electrical transport properties in section 3, revealing the variations of band structure and electronic structure due to pressure. Additionally, the microstructural imperfections correlated with pressure are summarized in section 4, suggesting that pressure can effectively manipulate microstructural evolution. Finally, section 5 is focused on a discussion of the relationship between pressure and thermal conductivity, particularly in lattice thermal conductivity (the contribution of pressure to the scattering mechanisms of phonons). On the basis of the summaries, an outlook is suggested that is to rationally employ pressure improving thermoelectric performance, the review furthermore enriches the understanding and conception of transport mechanisms and provides a bright strategy for thermoelectric investigations.

2. Crystal structure & pressure

The crystal structure is a basic cell that determines the transport properties of electrons and phonons, consequently influencing the thermoelectric performance of materials. The structural transformations, basically involving phase transition, cell volume, lattice parameters, and orientation, could be triggered by fundamental thermodynamic variables and are a major approach to improve thermoelectric transport properties. During a process of pressure performing a physical

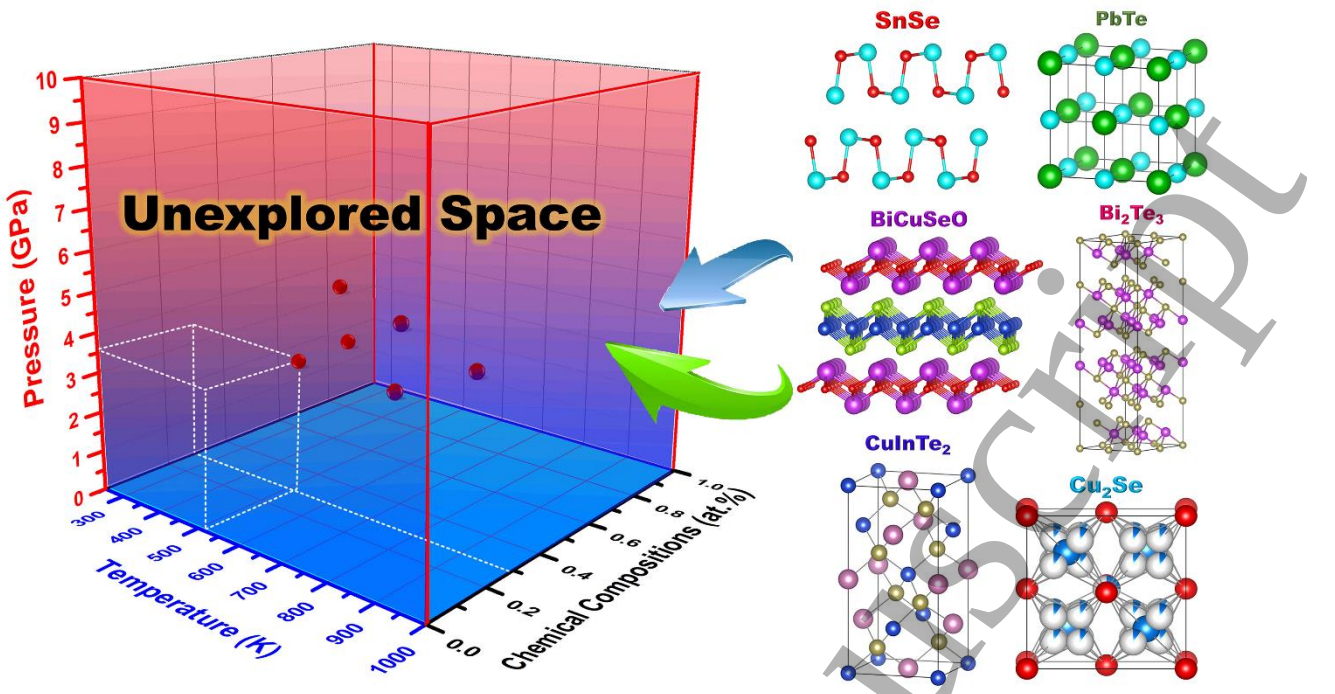

Figure 1. Schematic diagram of 3D unexplored space for thermoelectric materials, it is constituted by fundamental thermodynamic variables including pressure, temperature, and chemical compositions.

Table 1. The improved transport properties caused by pressure in various thermoelectric materials.

Materials	Type	S ($\mu V/K$)	S_P ($\mu V/K$)	Rate (%)	σ (10^{-6} S/m)	σ_P (10^{-6} S/m)	Rate (%)	Ref.
Ag_2Te	n	-0.14	-39.01	+28143.36	935.22	1828.55	+195.52	[28]
BiSb [a]	n	--	--	--	593.28	2015.40	+339.70	[29]
$BaBiTe_3$	p	201.12	319.20	+158.71	9.96	114.90	+1154.18	[30]
BiCuSeO	p	--	--	--	1.03	1.46	+142.13	[31]
α-Cu_2Se	p	56.32	68.45	+121.54%	719.42	847.46	+117.80	[32]
$Sb_{1.5}Bi_{0.5}Te_3$	n	-221.09	-317.19	+143.46	9.95	33.54	+336.892	[30]
SnSe	p	--	--	--	0.0021	23.95	+1156602.29	[34]
PbTe [b]	p	--	--	--	11.9	3658.02	+30729.58	[33]
PbTe [c]	p/n	247.52	-236.28	--	0.58	1.58	+275.21	[30]
PbTe	n	-116.35	-160.51	+137.95	0.51	2.51	+490.50	[30]
$Pb_{0.55}Te_{0.45}$ [c]	p/n	136.06	-221.46	--	0.51	1.58	+308.10	[30]
$Pb_{0.393}Sn_{0.157}Te_{0.45}$	p	--	--	--	0.76	1.86	+246.58	[30]
Ti_2O_3	n	-15.63	-39.21	+250.92	1.00	3.53	+350.94	[36]
$Nd_{0.45}Ce_{2.55}$-Pt_3Sb_4	p	84.77	291.24	+343.58	93.7	164.13	+175.14	[35]

S and σ are initial transport properties of materials at ambient condition or low pressure; S_P and σ_P are improved transport properties under high pressure (~GPa). [a] With increasing pressure, the carrier concentration of BiSb increases by 88 %, the carrier mobility meanwhile increases from 0.34×10^3 to 3.64×10^3 $cm^2V^{-1}S^{-1}$; [b] The thermal conductivity of PbTe decreases from 2.3 to 1.58 W/m/K with increasing pressure; [c] The conduction types are changed under pressure (~GPa).

compression on substances with unchanged composition and temperature, numerous materials show a structural evolution [42, 43]. In view of pressure-induced evolution, it is summarized as follows: The structural deformation, involving lattice parameters and lattice distortion, is supposed to be an initial response owing to the gentle shifting of atomic sites caused by pressure. An extreme case, *i.e.* phase transition, would be introduced by continually elevating pressure to a higher magnitude. The atomic sites are modified radically, thus leading to the destruction and reorganization of interatomic bonding and generating a metastable or stable structural configuration [44-47]. Such variations immediately motivate the changes in interatomic electrostatic interactions, electronic orbitals, and chemical bonding, which are responsible for the transport behaviors of electrons and phonons. For this reason, it is concluded that pressure is an effective tool to tune the electrical and thermal transport properties, promisingly realizing an enhancement in the zT value of thermoelectric materials.

In consideration of previous studies, we rationally divided the influence of pressure on crystal structure into three branches, those are lattice parameters, distortion, and phase

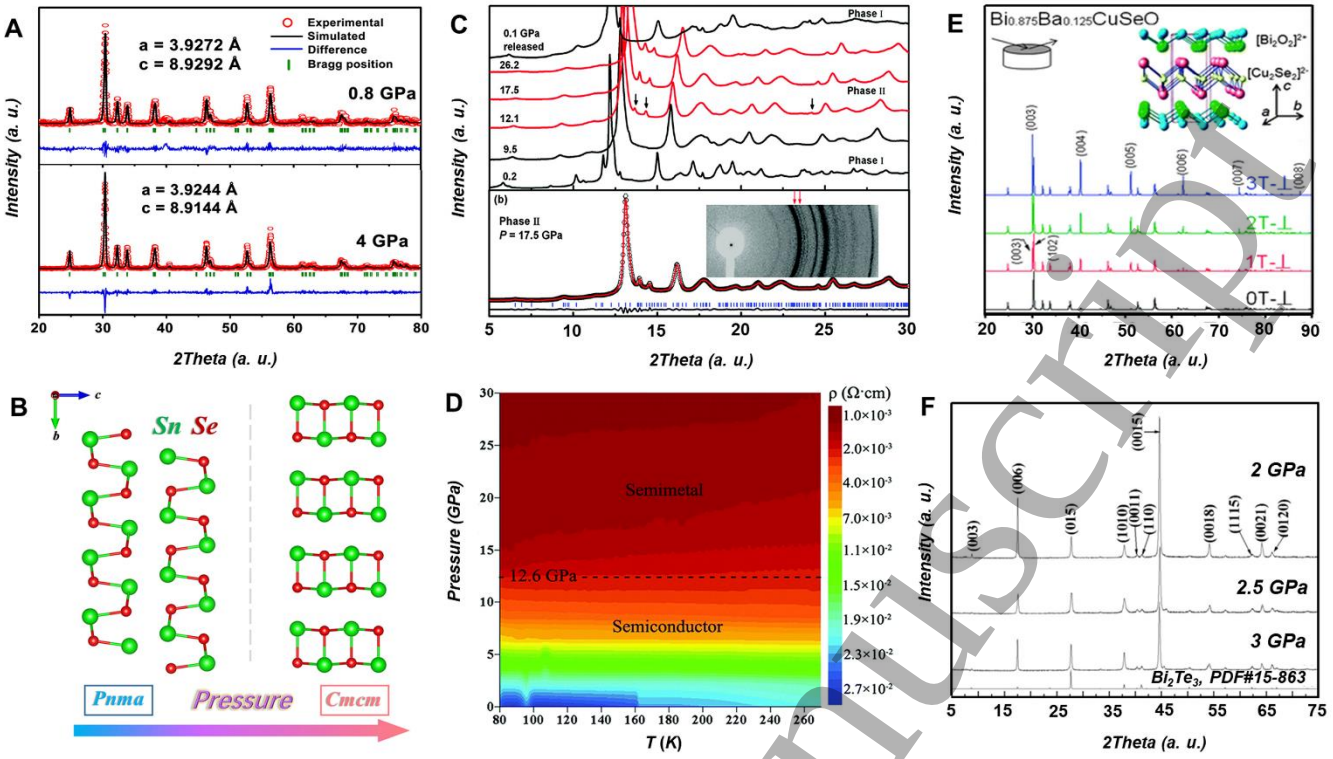

Figure 2. (A) Rietveld refinement were performed using XRD data of BiCuSeO synthesized at 0.8 and 4 GPa to achieve corresponding lattice parameters [48]. (B) The structural configurations of SnSe induced by pressure [49]. (C) XRD patterns of SnSe under different pressures corresponding to D [50]. (D) The transformation of the conductive behavior with increasing pressure in SnSe [50]; The strengthened (00l) orientation of BiCuSeO (E) and Bi_2Te_3 (F) caused by the application of pressure [51, 52].

transition. It is evident that interatomic spacing in crystals can be compressed under high pressure, leading to a reduction in lattice parameters (*a*, *b*, *c*) and in turn a shrinkage happened in cell volume [53], particularly for the in-situ high-pressure technology[47, 54, 55]. Besides, a lattice shrinkage was observed in materials after employing the high-pressure and high-temperature (HPHT) method as well, which was ascribed to a rapidly high-pressure quenching (HPHT process) freezing decreased lattice parameters to ambient conditions[56-58]. For instance, the Rietveld refinement of XRD data of BiCuSeO prepared *via* HPHT indicated that lattice parameters (*a*, *c*) showed a slight decrease with increasing synthesis pressure from 0.8 to 4 GPa (Figure 2A) [48]. The analogous cases are observed frequently in Bi_2Te_3, PbTe, SiGe, *etc*., indicating that HPHT, similar to *in-situ* high-pressure technology, could decrease lattice parameters by applying pressure accompanied by quenching treatment [59-61]. The application of pressure forces atomic movements in the direction of the $(\vec{h}, \vec{k}, \vec{l})$ vector, consequently influencing lattice parameters and atomic interaction. Compared to pristine axial orientation, the compression of interatomic spacing gives rise to the lattice distortion in the structural framework, which is recognized as a contribution on the reduction of lattice thermal conductivity [62]. With further increasing pressure, the crystal structure is going to be a phase transition accompanied by the destruction and reconstruction of interatomic chemical bonds, which is identified as another evolution stage in the structural transformation, showing a new structural configuration and fresh transport properties [37]. Recently, SnSe-based alloys have attracted extreme attention as the state-of-the-art thermoelectric materials [63]. An investigation indicated that SnSe possessed an intrinsic orthorhombic structure, while it would undergo a phase transition from Pnma to Cmcm phases under pressure (Figure 2B) [49, 64, 65]. Compared to Pnma phase, pressure-induced Cmcm phase presents a higher structural symmetry [17], which can give rise to a reduction of the deformation potential (Ξ) in SnSe. Such decreased Ξ is a symbol of mitigating the electron-phonon coupling [50] and beneficial to synergistically improve the electrical and thermal transport properties, enhancing the thermoelectric performance of SnSe-Cmcm. Moreover, the carrier concentration and mobility increase drastically in SnSe, when pressure is beyond 12GPa. A significant decrease in electrical resistivity is motivated, as can be seen in Figure 2C,D [50], which originates from a transformation in the conductive behavior from semiconductor to semimetal (or metal), its essential reason is a pressure-driven structural transition from an orthorhombic to a monoclinic system [66]. Given these cases, one can be told that the transport behavior is extremely dependent on spatially structural configurations. The solid evidences have confirmed that pressure is an effective and

feasible strategy to manipulate lattice parameters, disorder, dislocation, and phase transition, therefore driving fantastic transport properties. In other words, the thermoelectric transport properties could be modulated by the influence of high pressure on structural transformation. Furthermore, the application of pressure introduces an evident strengthening in the crystalline orientation, this phenomenon has been observed in lots of materials prepared under pressure [67, 68]. It can be imagined reasonably that the introduction of pressure shrinks interatomic spacing and strengthens binding energy among the atoms [69], consequently attracting abundant atoms to be arranged along with pressure direction during the preparation process. For this reason, the pressure-driven atoms are stacked periodically constructing specific crystal planes, which are arranged in the same direction finally forming the preferred orientation. Such orientated growth correlated with pressure has been observed and readily occurred in layered structural materials. Particularly, the pressure-driven orientation follows the growth of the (00l) planes (Figure. 2E,F) [51, 52], which is primarily attributed to the van der Waals forces in *c*-axis that are influenced by applied pressure, leading to the aggregation of atoms to form the (00l) planes. With regard to optimized crystalline orientation in layered thermoelectric materials, the electrical transport properties, particularly for carrier mobility, are generally boosted, thus achieving an improvement in thermoelectric performance [70].

3. Electrical transport properties influenced by pressure

The electrical transport properties are considered as the macroscopic performances of complicated electronic behaviors, and its nature is a response corresponding to the interaction among free electrons, consequently leading to a variation in band/electronic structure and in turn influencing the Seebeck coefficient (*S*) and electrical conductivity (σ) of thermoelectric materials. The power factor (*PF*) is a direct characterization reflecting the electrical transport properties of thermoelectric materials, as determined by $PF = S^2\sigma$. Long-term efforts found that some strategies could effectively improve the electrical transport properties, such as band convergence [71, 72], band alignment [73, 74], resonant level effect [75, 76], energy filtering effect [77, 78], *etc*. With the development of high-pressure technology, recent studies indicate that pressure, as a thermodynamic variable, is a unique approach to optimize the electrical transport behaviors, which has been proved in various thermoelectric materials involving SnSe-based alloys [79], PbTe-based alloys [80], Bi_2Te_3-based alloys [81], BiCuSeO-based alloys [82], *etc*.

3.1. Seebeck coefficient

Seebeck coefficient is a crucial parameter in the electrical transport properties and is defined readily on the basis of the single parabolic band (SPB) model as below [83]:

$$S = \frac{8\pi^2 k_B^2 T}{3eh^2} m_d^* \left(\frac{\pi}{3n}\right)^{2/3} \quad (1)$$

where k_B is the Boltzmann constant, $\hbar$ is the Planck's constant, m_d^* is the density-of-state effective mass, and n is the carrier concentration. The formula indicates that the Seebeck coefficient is determined primarily by tunable m_d^* and *n*, which are strongly associated with the electronic and band structures. Inspiringly, the application of pressure can motivate a variation in the electronic structure, more specifically involving the conduction/valence bands, band convergence, band dispersion, *etc.*, realizing a manipulation of the effective mass near the Fermi level. This actually means that the application of pressure provides a promising approach to the modulation of the Seebeck coefficient. According to the report of Li *et al.*, Al-doped Mg_2Si prepared by spark plasma sintering showed that a pressure could modulate the conduction band minimum (CBM), triggering band convergence in the CBM and then motivating a greater m_d^* (Figure 3A,B). A triple degeneracy in the CBM was obtained at 3 GPa and accompanied by a maximum m_d^* in $Mg_{1.97}Al_{0.03}Si$, which was favorable for the improvement of the Seebeck coefficient [84]. The analogous studies suggested that the electronic structure of degenerate n-type Bi_2S_3 materials showed evident dependency on pressure. The m_d^* increases initially with increasing pressure up to 7.2 GPa, consequently resulting in an enhancement in the Seebeck coefficient, while the m_d^* turns to degenerate when pressure is beyond 7.2 GPa, in contrast to the former, which results in an opposite effect on the Seebeck coefficient. Besides, Zhao *et al.* predicted a change in the electronic structure of Bi_2Te_3 under pressure of 0 ~ 6 GPa based on the first-principle calculations and Boltzmann transport theory [85]. The results suggested that the m_d^* increased sustainability as pressure went up. An anomalous variation appeared at 3 GPa in the Seebeck coefficient, which was attributed to extraordinary m_d^* caused by a change in band dispersion at v_1 and v_2. In addition, the bandgap is an essential factor in band structure and considered to possess a tight affiliation with carrier concentration, as shown in the formula below.

$$n = (Nc \cdot Nv)^{\frac{1}{2}} e^{\left[-\frac{Eg}{2kT}\right]} \quad (2)$$

where *n* is the carrier concentration, E_g is the bandgap, *k* is the Boltzmann constant, *T* is the temperature, *Nc* and *Nv* is the degeneracy of conduction/valence bands near the Fermi level, respectively. Combining the *equ.* (1) and (2), it readily concludes that a rational broadening of the bandgap is beneficial to the Seebeck coefficient. Fortunately, the change of the bandgap has been confirmed that could be manipulated *via* applying pressure [86-89], which implies that pressure could be employed to tune the Seebeck coefficient through the bandgap. Considering the role of pressure on the band

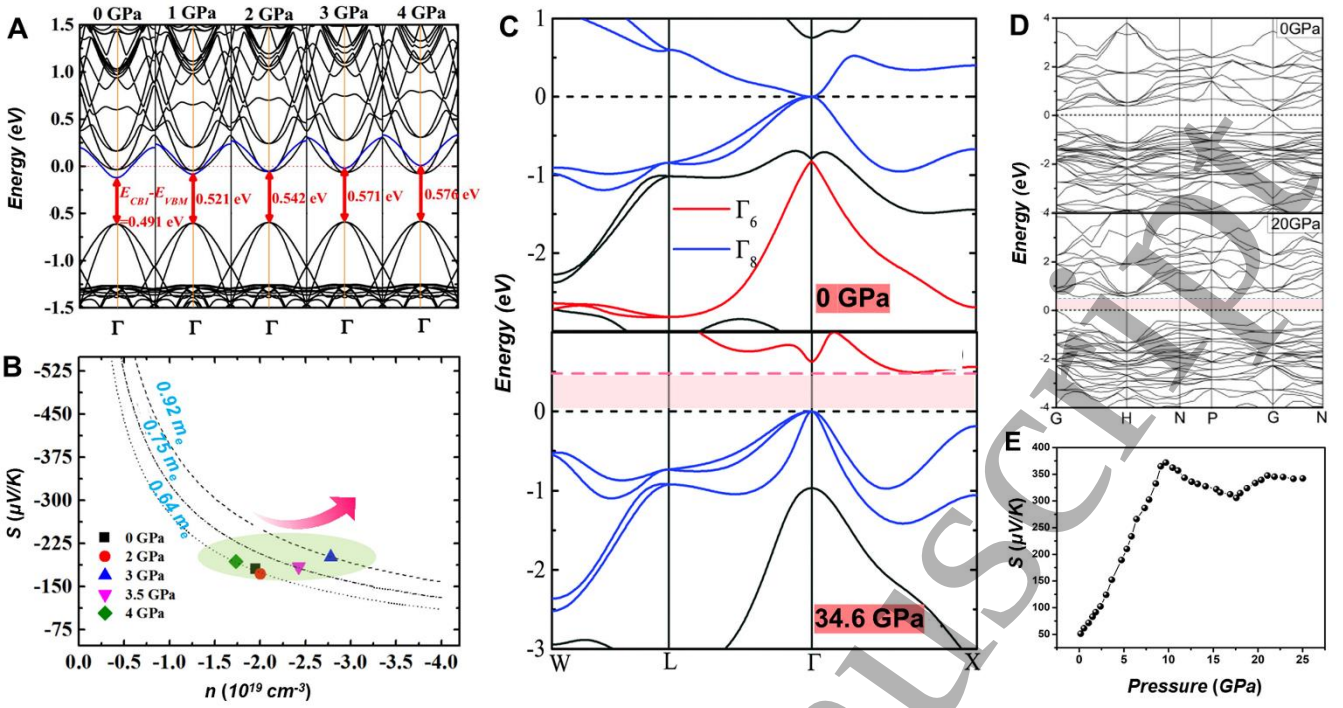

Figure 3. (A) Band structures of the $Mg_{63}AlSi_{32}$: Evolution of band structures with increasing pressure, the distance between the blue band and VBM increases as the pressure increase, Fermi level is set to 0 eV [84]. (B) Pisarenko plot (*S*~*n*) at room temperature of $Mg_{1.97}Al_{0.03}Si$ samples synthesized under different pressures [84]. (C) Band structures of LaPtBi under 0 and 34.6 GPa. The Fermi level is set at 0 eV [90]. (D) The calculated band structure of $CoSb_3$ at 0 and 20 GPa. The bandgaps for 0 and 20 GPa are 0.189 eV and 0.514 eV, respectively. The direct band semiconductor of $CoSb_3$ meanwhile changes to indirect band semiconductor due to pressure [62]. (E) Pressure dependent Seebeck coefficient (S) of $CoSb_3$ at room temperature [62].

structure, the half-Heusler compounds, *i.e.* LaPtBi, exhibited a variation in bandgap from a direct to an indirect gap due to pressure, leading to an increase in the Seebeck coefficient owing to the broadening of bandgap (Figure 3C) [90]. Similarly, $CoSb_3$ showed a transformation in bandgap with pressure from 0 to 20 GPa as that of LaPtBi [62, 91]. The mechanism has been elaborated by Wu *et al* [62], that is, the intensity of the electronic coupling and hybridization is strengthened gradually as the pressure increases, which makes the valence and conduction bands diffuse. As can be seen obviously in Figure 3D,E, with an increase of pressure, the high-energy valence bands broaden significantly and the conduction bands widen slightly away from the Fermi level, leading to an increase in bandgap of $CoSb_3$ and a sharp increase in the Seebeck coefficient. In contrast to a broadening of the bandgap induced by pressure, a reduction in the bandgap, which was achieved from an indirect to direct gap, was observed at 50 GPa in LiScGe alloys [92]. The finding suggests that the VBM and CBM approach to each other with pressure, the VBM transfers to a higher energy level, the CBM however shifts to a lower energy level. For the V_2VI_3-based thermoelectric materials with an intrinsic indirect gap, such as Bi_2Te_3, Sb_2Te_3, $BiSbTe_3$, Bi_2Te_2Se, *etc*, the BoltzTraP calculations predict a sequential decrease in the bandgaps with increasing pressure [93]. In the study of Bi_2Te_3 alloys, the pressure-induced bandgap shows an evident reduction, which is consistent with the prior prediction and triggers the transport of bipolar carriers, consequently degenerating the Seebeck coefficient in p-type Bi_2Te_3. However, although n-type Bi_2Te_3 exhibits a bipolar transport under high pressure, it remains to be expected to grab a higher Seebeck coefficient due to an increased DOS in the conduction bands [93]. Based on the mentioned above, applying pressure to tune the Seebeck coefficient should pay attention to the threshold of applied pressure and the bandgap property. These will influence the modulated results of pressure on the Seebeck coefficient. Such a diversity in the Seebeck coefficient *vs.* pressure may originate from the atomic sites, interatomic bonding, electronic orbitals, and electronegativity in various thermoelectric materials [31, 94]. The views remind us that it is an effective pathway to rationally employ pressure improving the Seebeck coefficient.

3.2 Electrical conductivity

Electrical conductivity is another critical parameter in the electrical transport properties. Impurity doping is a regular and effective strategy to improve the electrical conductivity of semiconductor materials, which is attributed to the influence of dopants on carrier concentration and electronic structure. The antisite defects or vacancies would be incorporated into the matrix as the impurity doping is performed, its function is to optimize carrier concentration in order to improve the

electrical conductivity. In addition to doping, pressure can produce mechanical deformation introducing the charged defects (antisite defect and vacancy) into the matrix, such cases are ordinarily accompanied by a manipulation of the carrier concentration. In the studies of Bi_2Te_3-based alloys, the findings suggest that the carrier concentration is strongly associated with the point defects including Bi'_{Te}, V'''_{Bi}, and $V^{\cdot\cdot}_{Te}$, which are responsible for supplying extra carriers [95]. The mechanical deformation formed by a high-strength compression is a typical case that incorporates various charged defects, which give rise to the donor-like effect influencing the carrier concentration in Bi_2Te_3-based alloys, as described in the following *equ.* [96, 97].

$$2V'''_{Bi} + 3V^{\cdot\cdot}_{Te} + Bi'_{Te} = V'''_{Bi} + Bi^{\times}_{Bi} + 4V^{\cdot\cdot}_{Te} + 6e'$$

it indicates that each equation offers six additional electrons as an important source of carriers, which not only can achieve a transition from p- to n-type conductive behavior (Figure 4A), but also can increase the electrical conductivity substantially in n-type Bi_2Te_3-based alloys [98]. Likewise, the electron concentration of as-melted p-type $Bi_2Te_2Se_1$ alloys was described approximately, as shown in the following relationship:

$$e \approx 2V^{\cdot\cdot}_{Se} + 2V^{\cdot\cdot}_{Te} - Bi'_{Se} - Bi'_{Te} \approx 0$$

which suggests that no extra electrons are supplied due to the annihilation of hole and electron carriers from antisite defects (Bi'_{Se}, Bi'_{Te}) and vacancies ($V^{\cdot\cdot}_{Se}, V^{\cdot\cdot}_{Te}$), respectively. However, the electrical conductivity will present an obvious reduction and even a transition in the conductive behavior from p- to n-type in the $Bi_2Te_2Se_1$ compounds, when the $Bi_2Te_{3-x}Se_x$ system is compressed introducing extra point defects. The result is attributed to the contribution of the donor-like effect caused by pressure-induced point defects [99].

On the other hand, the band engineering is available for tuning the carriers to improve the electrical conductivity [100-102]. As we mentioned in the former, *i.e.* pressure *vs.* Seebeck coefficient, the band engineering can be performed through applying pressure, which imply that the carrier concentration and mobility present a dependency on pressure. Theoretically, a first-principles study illustrates that the degeneracy of valence bands increases at Σ-L-Z-η in r-GeTe, when applied pressure increases to 5 GPa (Figure 4B,C). The m_d^* decreases significantly owing to a pressure of 5 GPa, and the degenerated valleys have a positive contribution to the transport of electrons. The decreased m_d^* together with degenerated valleys, which both originate from applied pressure, is favorable for improving carrier mobility, boosting an enhancement in the electrical conductivity (Figure 4D,E) [103]. Besides, the analogous case, that is increased carrier concentration caused by pressure-induced band degeneracy, was observed in Mg_2Sn, which gives rise to an enhancement in the electrical conductivity [104]. Considering the modulation of pressure on carrier mobility, the studies found that the application of pressure realized a conversion between the heavy and light bands in the electronic structure of $SiTrO_3$ (Figure 4F), which was ascribed to a pressure-induced structural transformation driving a subtle rearrangement of electrons. As a result, the carrier mobility was raised by ~ 300 % compared with that of pristine one without pressure, which extremely increased the electrical conductivity [105]. As for the effect of high-pressure sintering, the Te-doped BiCuSeO prepared by HPHT method likewise exhibits a dramatic enhancement in carrier mobility due to pressure [106]. The study suggests that the light hole (LH) band shifts to the high energy closing to the band edge with the effect of pressure, in contrast to the heavy hole (HH) band which is almost unchanged. The pressure-induced conversion in LH and HH bands motivates more electronic pockets contributing to the transport of electrons, finally achieving an improvement in electrical conductivity.

In addition to carrier concentration and electronic structure, the carrier scattering is supposed to be another factor influencing the electrical conductivity, the relationship is described according to the equation below.

$$\sigma = \tau e^2 n/m_d^* \quad (3)$$

where e is the elementary charge, n/m_d^* is determined by carrier concentration and electronic structure, and τ is the relaxation time and is related to the scattering mechanism (λ). It can be concluded that electrical conductivity is strongly associated with the scattering mechanisms, the affiliation originates from the relationship between carrier mobility and relaxation time ($\mu = \tau e/m_d^*$). Given the nondegenerate semiconductors, it is well known that the carrier mobility and scattering mechanism present an exponential relationship, which is expressed as $\mu \sim T^{\lambda}$, where λ = -3/2 is the acoustic phonon scattering [107], λ = 0 is the alloy scattering [108], and λ = 3/2 is the ionized impurity scattering [109]. The scattering mechanisms, similarly in the aforementioned factors, can also be tuned *via* pressure. In previous work, Liu *et al.* indicated that the implementation of pressure makes acoustic phonon scattering tend to alloy scattering in Te-doped BiCuSeO matrix, weakening carrier scattering and generating ultrahigh carrier mobility to enhance the electrical conductivity significantly [106]. Furthermore, p-type Mg_3Sb_2 exhibited the rate of electron scattering suppressed near the edge of the VB at 5 GPa, which suggested that the electron-phonon interaction is mitigated, thus being beneficial to improve the electrical conductivity [110]. Oppositely, by applying pressure on the Sb_2Te_3 thin film, the carrier mobility shows a slight deterioration due to strengthened interface scattering contribution to carrier transport. The result is primarily attributed to pressure-induced reduction in grain size increasing the density of grain boundaries [111]. Despite it's not an ideal sign what we are expected, such a case indeed exhibits the influence of pressure on the carrier scattering. On the basis of all the investigations above, we could summarize that applying pressure to modulate the *n* (the carrier

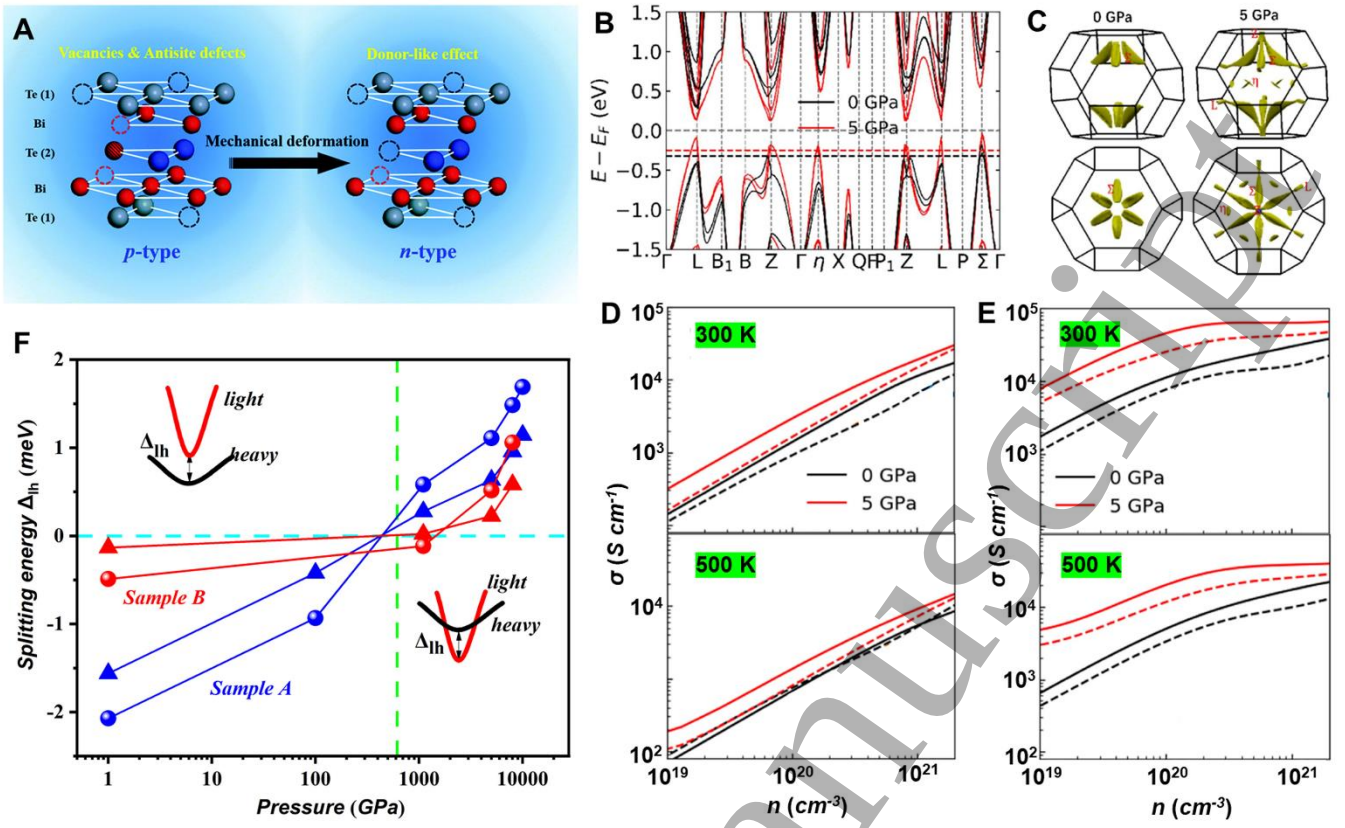

Figure 4. (A) Schematic view of the point defects. Balls in red, grey and blue stand for the atoms of Bi, Te(1) and Te(2), respectively. Empty circles denote vacancies and red balls with slash are representatives of antisite defects Bi'_{Te} [98]. (B) Electronic band structure of r-GeTe along high-symmetry paths at different pressures, the corresponding Fermi surfaces are shown in (C) [103]. Electrical conductivity as a function of hole concentration calculated with the CRTA (D) and the EPW (E) package for p-type r-GeTe [103]. (F) Pressure dependence of Δ_{lh} in sample A (blue) and sample B (red) at T = 5 K is calculated, Δ_{lh} is the energy splitting between light and heavy bands [105].

concentration), m_d^* (the electronic structure), and τ (the scattering mechanism) is a potential pathway to modify the electrical conductivity, achieving an optimization of the electrical transport properties.

4. Microstructural evolution with pressure

Microstructure as an observable characteristic is used to intuitively analyze the effect of external factors on the grain sizes, orientation, and lattice defects of thermoelectric materials, in order to figure out its contribution to the transports of carriers and phonons, especially in lattice thermal conductivity. The unique physical parameter, "pressure", has confirmed a significant influence on the texture (SEM observation) and lattice structure (HRTEM observation) [112-114]. With regard to the textural feature, we generally concern the effect of pressure on the grain sizes, boundaries (interfaces), and orientation. For compressed structural features, it needs to be clarified that the results applied by repeated pressure (with the same order of magnitude) are different from that of increased pressure during the synthesis process. Two-type results indicate completely opposite changes in grain sizes [5, 115, 116]. Apparently, the nucleation centers of grains are compressed continuously with increasing pressure, restricting the spaces of grain growth and thus leading to a reduction in grain sizes. Such pressure-induced reduction in grain sizes is observed in various thermoelectric materials [117-120]. For instance, Deng *et al.* reported that $CoSb_3$-based alloys, as shown in Figure 5A,B [121], were synthesized under different pressures (~GPa), the observation found that the grain sizes exhibited a significant decrease with increasing pressure. The analogous situation occurs in the synthesis of polycrystalline SnSe as well [122], in contrast with the former, the magnitude of pressure is ~MPa level applied in the preparation process of SnSe, which is far less than ~GPa level. This suggests that the effect of increased pressure on grain sizes may be universal no matter whether of ~MPa or ~GPa level. In view of the pressure-induced cases above, it can rationally conclude that the shrinkage of grain sizes is accompanied by an enhancement in grain boundaries (interfaces). In contrast, multiple compression with the same order of magnitude (*i.e.* thermal deformation) is supposed to be an inducement that facilitates grain growth in materials with layered structure [123, 124]. The enlarged grains strengthen the textural structure along a crystal axis. Interestingly, these two-type pressures both observe the ordered arrangement of crystal planes (texture strengthening)

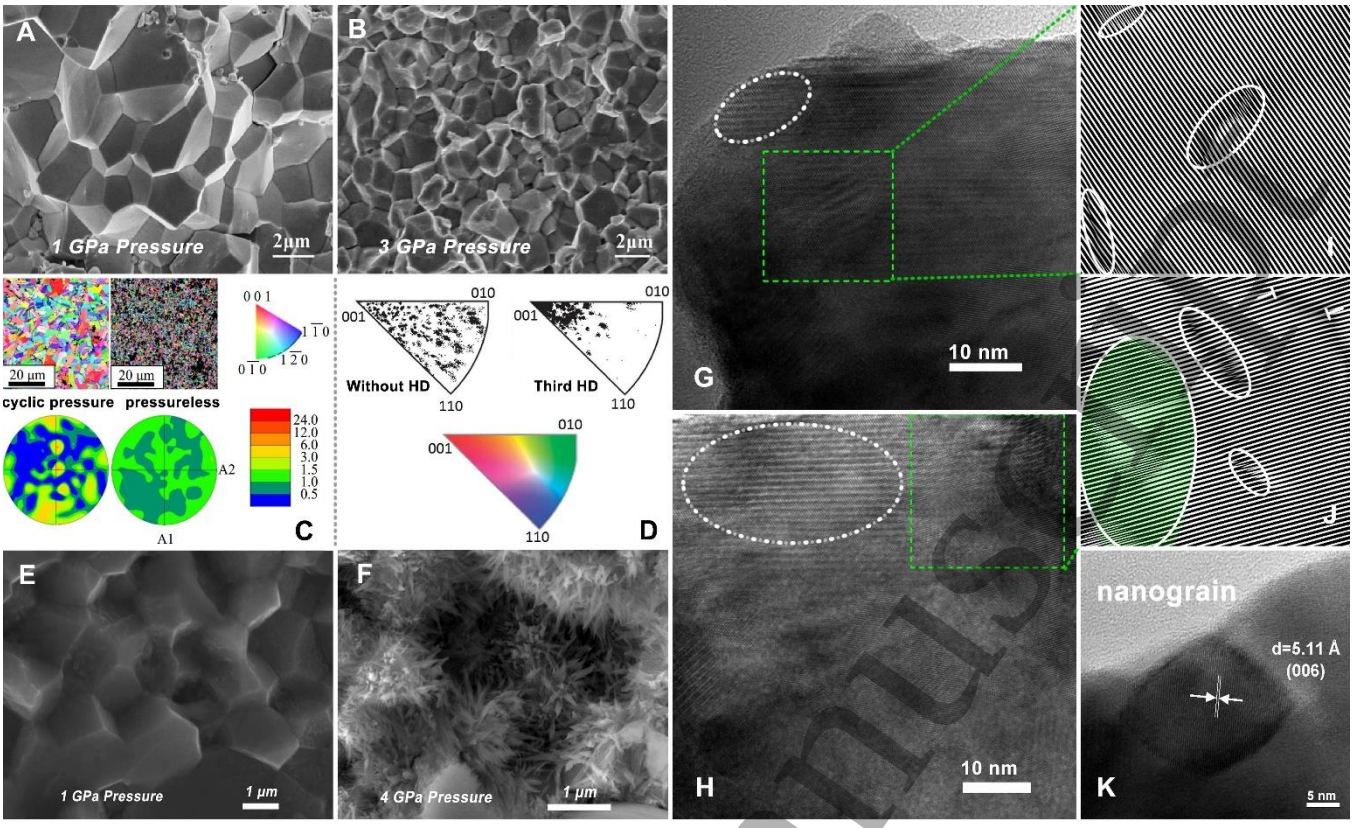

Figure 5. SEM images of $Ba_{0.05}In_{0.15}Co_4Sb_{11.5}Te_{0.5}$ synthesized under 1 GPa (A) and 3 GPa (B) [125]. (C) Inverse pole figures of $Bi_{0.4}Sb_{1.6}Te_3$ (measured surface perpendicular to pressure direction) prepared with cyclically constant pressure and without pressure [126]. (D) Inverse pole figures of $Bi_{0.875}Ba_{0.125}CuSeO$ (measured surface perpendicular to pressure direction) synthesized without hot forging and with third hot forging using constant pressure [51]. SEM images of $Ba_8Cu_6Si_{40}$ prepared under 1 GPa (E) and 4 GPa (F) [127]. HRTEM images of $Bi_{0.5}Sb_{1.5}Te_3$ synthesized at 1 GPa (G) and 3.2 GPa (H). IFFT images of (I) and (J) corresponding to the rectangular regions in (G) and (H), respectively [128]. (K) HRTEM image of a nanograin from the $Bi_{0.5}Sb_{1.5}Te_3$ prepared under high pressure [128].

in Bi_2Te_3 and BiCuSeO-based materials (Figure 5C,D) [126]. The ordered arrangement has been elaborated in section 2 according to the crystal structure. In addition, Sun *et al.* showed that implementing pressure during the synthesis process of $Ba_8Cu_6Si_{40}$ not only can manipulate grain sizes, but can change the surface morphology of grains (Figure 5E,F) [127]. The researchers claimed that pressure-induced changes were rare happened in surface characteristics of grains, it might need to be investigated further to reveal the intrinsic mechanism of pressure modulating the surface crystallization. In our opinion, it should be identified as an oversaturation caused by the effect of increased pressure, triggering extensive segregation in the surfaces. Although the $Ba_8Cu_6Si_{40}$ synthesized at 3GPa performed an EDS measurement to clarify the compositions of different spots in matrix, the results cannot match well with the nominal composition of $Ba_8Cu_6Si_{40}$, let alone the sample synthesized at 4GPa (with more surface crystallization). On the contrary, the EDS measurement shows Cu- and Si-deficiencies and discrepant compositions in measured spots, which exactly demonstrate our perspective above, *i.e.* the pressure can introduce an oversaturation. Anyway, the variation in grains indeed increases the surface areas because of pressure rise, leading to an enhancement in the density of grain boundary.

Defects are relevant strongly to the transport of carriers and phonons as a critical characteristic in microstructure, it can be divided into polytype defects according to the scale differences, involving atomic scale (point defect and dislocation) [129-132], nanoscale (nanoparticle, stacking fault, and precipitate) [133-135], and meso/microscale (grain boundary and pore) [136]. As far as we're concerned in thermoelectrics, the type and amount of lattice defects possess significant influence on thermoelectric transport properties. The lattice defects literally incorporate imperfections with atomic scale and nanoscale in microstructure, the low-dimensional defects can be identified by HRTEM measurement. Pressure is considered as a practical approach that introduces local strain to generate typically structural modulations (Figure 5G,H) [128, 137], which form massive lattice defects such as irregularities, distortions, dislocations [138-141], *etc*. The investigations found that lattice distortions and dislocations performed an evident enhancement with increasing pressure (Figure 5I,J) [128], which was primarily attributed to strengthened strain fields caused by pressure rise during the synthesis process. In addition to lattice distortions

and dislocations, the point defects (vacancies and antisite defects) as low-dimensional defects can also be introduced by pressure, which has been elaborated in 3.2. Unexpectedly, a nanograin was achieved in Bi_2Te_3-based alloys fabricated by HPHT method, as shown in Figure 5K. The routine concept tends to express that high pressure gives rise to the densification and cannot form the nanocrystallization in microstructure, while the finding is firmly against the empirical concept. The reason is supposed to be that the overloaded pressure produces larger mechanical deformation in lattice structure, and it is accompanied simultaneously by an *in-situ* heat treatment (HPHT process), contributing to *in-situ* recrystallization in the location of lattice defects to constitute the nanoparticles. Overall, applying pressure to introduce and manipulate the defects is available, which means that pressure as an unconventional variable can be employed to design microstructural features.

5. Relationship between thermal conductivity and pressure

Thermal conductivity symbolizes a capacity of the heat conduction in solids and is constituted by the lattice thermal conductivity (κ_{lat}) and the electronic thermal conductivity (κ_{ele}), as expressed by $\kappa_{tot} = \kappa_{lat} + \kappa_{ele}$ [142], where the κ_{lat} is dependent on the phonon transport that is primarily determined by microstructure (*ca.* scattering mechanism). Due to independent κ_{lat} from the carrier concentration [143-145], it is identified as an effective pathway through manipulating imperfect architectures, such as point defect, dislocation, distortion, grain boundary, precipitate, *etc.*, to reduce the κ_{lat} without deterioration in electrical properties (it will be discussed in more details below) (Figure 6A), realizing an improvement in thermoelectric performance [146-148]. Such a strategy is still dominant for various materials to improve thermoelectric performance so far. On the other hand, the κ_{ele} can be calculated by the Lorenz parameter (L) and electrical conductivity (σ) corresponding to a specific temperature, *i.e.* $\kappa_{ele} = L\sigma T = LTne\mu$. Given the effect of pressure on the crystal structure, electrical transport properties, and microstructure, it is evident that the implementation of pressure definitely introduces an influence on total thermal conductivity caused by the changes of the κ_{ele} or the κ_{lat}.

Aiming to a reduction in κ_{lat}, the purpose of a microstructural modification is to increase various scattering mechanisms from multiscale defects, strengthening barriers for the transport of full-frequency phonons. On the basis of the classic Callaway model [149], the κ_{lat} can be determined by equation (4) involving the parameters, which symbolize the role of the scattering mechanisms.

$$\kappa_{Lat} = \frac{K_B}{2\pi^2 v}\left(\frac{K_B T}{\hbar}\right)^3 \int_0^{\theta_D/T} \frac{\chi^4 e^{\chi}}{\tau_c \left(e^{\chi}-1\right)^2} d\chi \qquad (4)$$

where χ is defined as $\hbar\omega/K_B T$, ω is the phonon frequency, θ_D is the Debye temperature, τ_c is the relaxation time, K_B is the Boltzmann constant, $\hbar$ is the Planck constant, and v is the phonon propagation velocity. The τ_c can be divided into various scattering processes in terms of intrinsic mechanisms.

$$\frac{1}{\tau_C} = \frac{1}{\tau_U} + \frac{1}{\tau_N} + \frac{1}{\tau_{PD}} + \frac{1}{\tau_D} + \frac{1}{\tau_B} + \cdots \qquad (5)$$

where τ_U, τ_N, τ_{PD}, τ_D, and τ_B describe the scattering mechanisms of acoustic phonon (Umklapp process), normal process, point defect, dislocation, and grain boundary, respectively. It is essential to mention that extra variables can be added in equation (5) when the scattering mechanisms increase, which is dependent on the microstructural evolution. Zhu *et al*. simplified an expression of the relationship among τ_C and other parameters, thereby linking up the τ_C and the ω (phonon frequency) [150].

$$\tau_C^{-1} = A\omega^4 + Bexp(-\theta_D/3T)T\omega^2 + C\omega^2 + \frac{v}{d}\omega^0 \qquad (6)$$

where *v/d* represents the scattering of grain boundary, and *A, B, C* are the prefactors for point defect scattering, Umklapp scattering, and electron-phonon scattering, respectively. This means that we could express different scattering mechanisms using a simple function, namely $\tau_i = X\omega^j$, herein X is fitting prefactors and j depicts the relationship of τ_i *vs* ω for different scattering processes. Moreover, the τ and ω correspond to the phonon wavelengths (λ), which are regarded to some extent as the defect scales (l), *i.e.* $\lambda \sim l$. Therefore, it makes sense that the microstructural modification accompanied by introducing multiscale imperfections and increasing densities of various defects can significantly decrease the κ_{lat}, thus improving thermoelectric performance. However, it should be noted that the high-dimensional defects with long l not only can scatter long-wavelength phonons, but scatter low-energy carriers, leading to degenerated carrier transport. Selectively introducing low-dimensional defects thus would be a key to reducing the κ_{lat} without deterioration in electrical properties.

Undoubtedly, the contribution of pressure on total thermal conductivity can be embodied in the κ_{ele} and the κ_{lat}. As abovementioned the κ_{ele} can be calculated readily using $\kappa_{ele} = L\sigma T$, which implies the major influences on the κ_{ele} originating from the electrical transport properties. In section 3, we have elaborated the modulation of pressure on electrical properties, which is applicable for guiding the optimization of pressure-induced κ_{ele}. Furthermore, the experimental κ_{lat} is estimated indirectly by subtracting the κ_{ele} from the κ_{tot}. To investigate the contribution of different scattering processes, the Callaway model is generally employed to fit the curve of lattice thermal conductivity, revealing the roles of various scattering mechanisms. Combined with the relationship of $\tau_i = X\omega^j$ and $\omega \sim \lambda \sim l$, the κ_{lat} is identified as a response from entire scattering processes, which suggests that the κ_{lat} could be manipulated by pressure introducing multiscale defects and increasing defect density. However, the issue faced is that the κ_{tot} is difficult to be characterized during the process of *in-situ*

high pressure, let alone the κ_{lat}. We therefore concentrate on the κ_{lat} of thermoelectric materials prepared under high

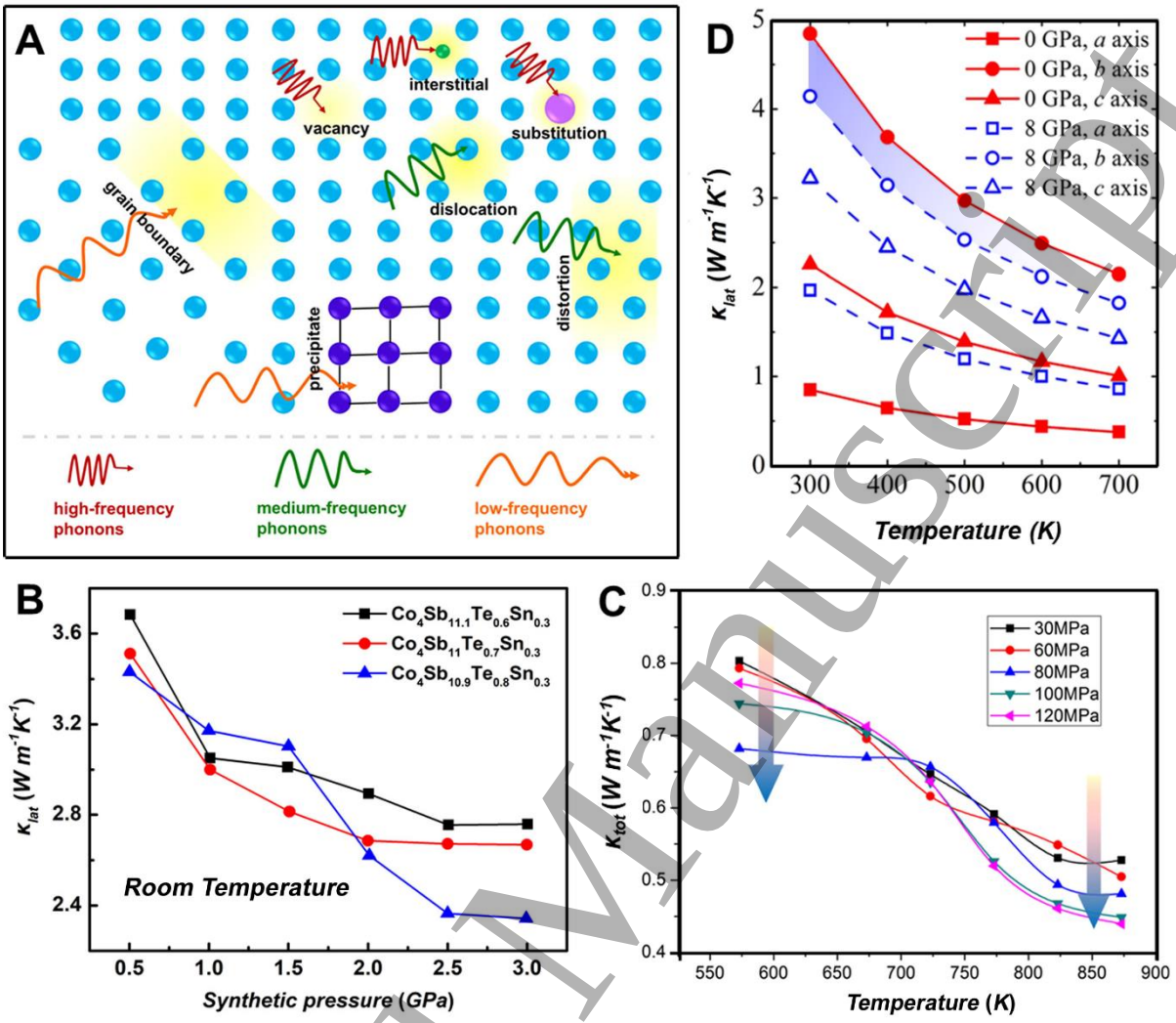

Figure 6. (A) Schematic diagram of the scattering mechanisms for the influence of multitype defects with different scales on high-, medium-, and low-frequency phonons. (B) The relationship between lattice thermal conductivity and synthetic pressure in $Co_4Sb_{11.7-x}Te_xSn_{0.3}$ at room temperature [57]. (C) Temperature-dependent thermal conductivity of polycrystalline SnSe under different pressures [122]. (D) The lattice thermal conductivity of GeSe along the *a*-, *b*-, and *c*-axis directions at two representative pressures from 300 to 700 K [151].

pressure (~GPa) rather than that of samples using *in-situ* high pressure. The HPHT method is exactly a preferred pathway to realize an investigation in the modulation of high pressure on the κ_{lat}. Using HPHT to fabricate a series of $CoSb_3$-based alloys, the κ_{lat} of reaction products exhibits a monotonous reduction with increasing synthesis pressure, as shown in Figure 6B [57], which is attributed to the enhancements in pressure-induced grain boundaries, lattice distortions, and dislocations strengthening the phonon scattering. Such behavior is observed as well in other thermoelectric species prepared by HPHT [86, 127, 152, 153]. Besides, Zhang *et al*. demonstrated that the magnitudes of pressure with ~MPa level was still available for decreasing κ_{tot} (κ_{lat}) in polycrystalline SnSe (Figure 6C) [122]. It is essential to note that the κ_{lat} possesses a characteristic of the anisotropy (Figure 6D) [151], which could be strengthened gradually with exerting pressure, particularly in materials with layered structure. In contrast to the abovementioned behavior of κ_{lat} *vs*. pressure, the κ_{lat} may increase in response to pressure rise in specific axial (or pressure) directions. With regard to anisotropic κ_{lat} corresponding to pressure, the desired κ_{lat} should be considered in a specific direction, which is to follow a decreased behavior with increasing pressure. In addition, the results of theoretical calculation suggest that an increased pressure could motivate a higher phonon frequency, a decrease in group velocity of phonons, and low heat capacities in materials [145], these optimizations in parameters correlated with pressure are favorable for a reduction in κ_{lat} as well. To sum up, the κ_{lat} can be manipulated by pressure to realize a desired decrease, which primarily originates from the

synergistic modulation of pressure on the electrical transport properties, multiscale defects, and thermodynamic parameters.

6. Summary and outlook

In the review, we summarize recent progress that is the influence of pressure on crystal structure, electrical transport properties, microstructure, and thermal conductivity in thermoelectric materials, and elaborate the manipulation of pressure on physical variables and its influences on transport properties. Besides, the remarkable advantages of pressure have been proposed including pressure-induced phase transition, band/electronic structure, defects, and low κ_{lat}, in which high-pressure phase transition is a fascinating subject for exploring potentially high-performance thermoelectric materials and deeply understanding the structure and transport properties of materials under high pressure. Moreover, as for existing thermoelectric systems, the layered structures, phase change materials (PCMs), and liquid-like compounds may be more suitable for high-pressure preparation and optimization due to their tuneable structures. Therefore, applying pressure as a unique tool to investigate and design thermoelectric materials gives an extreme possibility for driving a giant development in thermoelectrics.

Sustained efforts in high-pressure techniques make it possible for preparing large-volume thermoelectric materials under high pressure (from ~MPa to ~GPa level), which provides a prior condition for an improvement in thermoelectric performance. However, the preparation of large-scale samples under ultrahigh pressure (>10 GPa) remains a colossal challenge due to the limitation of a high-pressure equipment, in the meantime, the case also restricts the investigation of thermoelectric transport properties of samples prepared under ultrahigh pressure. By contrast, despite the experiment of *in-situ* high pressure (diamond anvil cell, DAC) can achieve higher pressure compared with the former, the approach is difficult to capture ultrahigh-pressure performance of samples and synthesize large-scale samples for further characterization and application at ambient conditions. In addition to the challenge above, there is another issue to be further resolved, that is, the theoretical data calculated cannot precisely corresponds to that of the experimental measurements. The case is primarily attributed to ideal physical models embedded in the software programs, which overlook some real conditions in the experiments, leading to a difficulty in describing high-pressure experimental processes. In summary, the high-pressure application faces new opportunities and great challenges in thermoelectrics. To figure out these issues, but not limited to those, it would be beneficial to the understanding of physical mechanisms in the modulation of pressure on structure and performance, ultimately increasing the *zT* values of existing thermoelectric materials or creating high-performance thermoelectric materials.

Acknowledgements

This work was financially supported by the Natural Science Foundation of Jilin Province (20200201254JC and 20200801006GH), the Education Department of Jilin Province (JJKH20220761KJ), and the "Program of Youth Talents" of Jilin Association of Science and Technology (181906). Prof. D.H.G. is acknowledged specially for his contribution to suggestions and modifications in Section 4.

Conflict of Interest

The authors declare no conflict of interest.

References

[1] Hinterleitner B, Knapp I, Poneder M, Shi Y, Muller H, Eguchi G, Eisenmenger-Sittner C, Stoger-Pollach M, Kakefuda Y, Kawamoto N, Guo Q, Baba T, Mori T, Ullah S, Chen X Q and Bauer E 2019 *Nature* **576** 85-90

[2] He W, Wang D, Wu H, Xiao Y, Zhang Y, He D, Feng Y, Hao Y J, Dong J F, Chetty R, Hao L, Chen D, Qin J, Yang Q, Li X, Song J M, Zhu Y, Xu W, Niu C, Li X, Wang G, Liu C, Ohta M, Pennycook S J, He J, Li J F and Zhao L D 2019 *Science* **365** 1418-1424

[3] Mao J, Zhu H, Ding Z, Liu Z, Gamage G A, Chen G and Ren Z 2019 *Science* **365** 495-498

[4] Hou C and Zhu M 2022 *Science* **377** 815-816

[5] Hu L P, Liu X H, Xie H H, Shen J J, Zhu T J and Zhao X B 2012 *Acta Materialia* **60** 4431-4437

[6] Gao W, Wang Z, Huang J and Liu Z 2018 *ACS Appl Mater Interfaces* **10** 18685-18692

[7] Hwang H and Jang K-S 2021 *Sustainable Energy & Fuels* **5** 267-273

[8] Jiang B, Yu Y, Cui J, Liu X, Xie L, Liao J, Zhang Q, Huang Y, Ning S, Jia B, Zhu B, Bai S, Chen L, Pennycook S J and He J 2021 *Science* **371** 830-834

[9] Zhu Q, Song S, Zhu H and Ren Z 2019 *Journal of Power Sources* **414** 393-400

[10] Shi X L, Zou J and Chen Z G 2020 *Chem Rev* **120** 7399-7515

[11] Chang C, Wu M, He D, Pei Y, Wu C F, Wu X, Yu H, Zhu F, Wang K, Chen Y, Huang L, Li J F, He J and Zhao L D 2018 *Science* **360** 778-783

[12] Venkatasubramanian R, Siivola E, Colpitts T and O'Quinn B 2001 *Nature* **413** 597-602

[13] Liu Z, Wang Y, Mao J, Geng H, Shuai J, Wang Y, He R, Cai W, Sui J and Ren Z 2016 *Advanced Energy Materials* **6** 1502269

[14] Tan X, Liu G-Q, Hu H, Shao H, Xu J and Jiang J 2019 *Journal of Materials Chemistry A* **7** 8922-8928

[15] Tan X, Wang L, Shao H, Yue S, Xu J, Liu G, Jiang H and Jiang J 2017 *Advanced Energy Materials* **7** 1700076

[16] Wu T, Chen X, Xie H, Chen Z, Zhang L, Pan Z and Zhuang W 2019 *Nano Energy* **60** 673-679
[17] Li C W, Hong J, May A F, Bansal D, Chi S, Hong T, Ehlers G and Delaire O 2015 *Nature Physics* **11** 1063-1069
[18] Dangić Đ, Hellman O, Fahy S and Savić I 2021 *npj Computational Materials* **7** 57
[19] Yang J, Zhang X Z, Liu G W, Zhao L J, Liu J L, Shi Z Q, Ding J N and Qiao G J 2020 *Nano Energy* **74** 104826
[20] Hu L P, Wu H J, Zhu T J, Fu C G, He J Q, Ying P J and Zhao X B 2015 *Advanced Energy Materials* **5** 1500411
[21] Qin B, Wang D, He W, Zhang Y, Wu H, Pennycook S J and Zhao L D 2019 *J Am Chem Soc* **141** 1141-1149
[22] Li H, Hayashi K, Nagashima Y, Yoshioka S, Dong J, Li J-F and Miyazaki Y 2021 *Chemistry of Materials* **33** 2543-2547
[23] Xiao G, Wang Y, Han D, Li K, Feng X, Lv P, Wang K, Liu L, Redfern S A T and Zou B 2018 *J Am Chem Soc* **140** 13970-13975
[24] Lv P, Sun Y, Sui L, Ma Z, Yuan K, Wu G, Liu C, Fu R, Liu H, Xiao G and Zou B 2020 *J Phys Chem Lett* **11** 920-926
[25] Mujica A, Rubio A, Muñoz A and Needs R J 2003 *Reviews of Modern Physics* **75** 863-912
[26] Mao H-k and Hemley R J 1994 *Reviews of Modern Physics* **66** 671-692
[27] Xiao G, Cao Y, Qi G, Wang L, Liu C, Ma Z, Yang X, Sui Y, Zheng W and Zou B 2017 *J Am Chem Soc* **139** 10087-10094
[28] Yuan B, Tao Q, Zhao X, Cao K, Cui T, Wang X and Zhu P 2014 *Rev Sci Instrum* **85** 013904
[29] Liu H, Wang J, Han Y and Gao C 2022 *Journal of Materials Chemistry C* **10** 3531-3537
[30] Ovsyannikov S V and Shchennikov V V 2009 *Chemistry of Materials* **22** 635-647
[31] Zhang Q, Chen C, Li N, Huang Q, He Y, Liu X, Wang B, Zhang D, Kim D Y, Wang Y, Xu B and Yang W 2018 *The Journal of Physical Chemistry C* **122** 15929-15936
[32] Zhao W, Cheng J, Wang D, You C, Zhang J, Ye M, Wang X, Dong S, Tao Q and Zhu P 2022 *Rev Sci Instrum* **93** 103901
[33] Zhu P W, Jia X, Chen H Y, Chen L X, Guo W L, Mei D L, Liu B B, Ma H A, Ren G Z and Zou G T 2002 *Chemical Physics Letters* **359** 89-94
[34] Chen X, Lu P, Wang X, Zhou Y, An C, Zhou Y, Xian C, Gao H, Guo Z, Park C, Hou B, Peng K, Zhou X, Sun J, Xiong Y, Yang Z, Xing D and Zhang Y 2017 *Physical Review B* **96** 165123
[35] Meng J F, Polvani D A, Jones C D W, DiSalvo F J, Fei Y and Badding J V 1999 *Chemistry of Materials* **12** 197-201
[36] Ovsyannikov S V, Wu X, Garbarino G, Nunez-Regueiro M, Shchennikov V V, Khmeleva J A, Karkin A E, Dubrovinskaia N and Dubrovinsky L 2013 *Physical Review B* **88** 184106
[37] Chen L C, Chen P Q, Li W J, Zhang Q, Struzhkin V V, Goncharov A F, Ren Z and Chen X J 2019 *Nat Mater* **18** 1321-1326
[38] Biesner T, Li W W, Tsirlin A A, Roh S, Wei P C, Uykur E and Dressel M 2021 *Npg Asia Materials* **13** 12
[39] Liu H, Wang J, Han Y H and Gao C X 2022 *Journal of Materials Chemistry C* **10** 3531-3537
[40] Yu H, Gao D, Wang X, Du X, Lin X, Guo W, Zou R, Jin C, Li K and Chen Y 2018 *NPG Asia Materials* **10** 882-887
[41] Li H, Wu K, Yang S, Boland T, Chen B, Singh A K and Tongay S 2019 *Nanoscale* **11** 20245-20251
[42] Roychowdhury S, Ghosh T, Arora R, Waghmare U V and Biswas K 2018 *Angew Chem Int Ed Engl* **57** 15167-15171
[43] Sarkar D, Ghosh T, Roychowdhury S, Arora R, Sajan S, Sheet G, Waghmare U V and Biswas K 2020 *J Am Chem Soc* **142** 12237-12244
[44] Zhang Y, Yan H, Song Q, Zhou Q, Li Z and Liu Y 2020 *Journal of Alloys and Compounds* **818** 152881
[45] Zhang Y, Shao X, Zheng Y, Yan L, Zhu P, Li Y and Xu H 2018 *Journal of Alloys and Compounds* **732** 280-285
[46] Ji D, Chong X, Ge Z-H and Feng J 2019 *Journal of Alloys and Compounds* **773** 988-996
[47] Calderón-Cueva M, Peng W, Clarke S M, Ding J, Brugman B L, Levental G, Balodhi A, Rylko M, Delaire O, Walsh J P S, Dorfman S M and Zevalkink A 2021 *Chemistry of Materials* **33** 567-573
[48] Liu Z, Guo X, Yu M, Wang D, Qin J, Jin F and Xue X 2020 *Journal of Alloys and Compounds* **812** 152106
[49] Alptekin S 2011 *J Mol Model* **17** 2989-2994
[50] Yan J, Ke F, Liu C, Wang L, Wang Q, Zhang J, Li G, Han Y, Ma Y and Gao C 2016 *Phys Chem Chem Phys* **18** 5012-5018
[51] Sui J H, Li J, He J Q, Pei Y L, Berardan D, Wu H J, Dragoe N, Cai W and Zhao L D 2013 *Energy & Environmental Science* **6** 2916-2920
[52] Guo X, Jia X, Jie K, Sun H, Zhang Y, Sun B and Ma H 2013 *Chemical Physics Letters* **568-569** 190-194
[53] Yang L T, Ding L-P, Shao P, Tiandong Y H, Zhao Z L, Zhang F-H and Lu C 2021 *Journal of Alloys and Compounds* **853** 157362
[54] Braun C, Borger S L, Boyko T D, Miehe G, Ehrenberg H, Hohn P, Moewes A and Schnick W 2011 *J Am Chem Soc* **133** 4307-4315
[55] Vogel S, Bykov M, Bykova E, Wendl S, Kloss S D, Pakhomova A, Chariton S, Koemets E, Dubrovinskaia N, Dubrovinsky L and Schnick W 2019 *Angew Chem Int Ed Engl* **58** 9060-9063
[56] Guo X, Jia X, Su T, Jie K, Sun H and Ma H 2012 *Chemical Physics Letters* **550** 170-174

[57] Sun H, Jia X, Deng L, Lv P, Guo X, Zhang Y, Sun B, Liu B and Ma H 2015 *Journal of Materials Chemistry A* **3** 4637-4641

[58] Chen Q, Ma H A, Li X J, Wang Y, Liu B M, Wang C X, Ji G Y, Wang J, Chang L J, Zhang Y W and Jia X P 2020 *Journal of Alloys and Compounds* **844** 156124

[59] Ovsyannikov S V, Shchennikov V V, Vorontsov G V, Manakov A Y, Likhacheva A Y and Kulbachinskii V A 2008 *Journal of Applied Physics* **104** 053713

[60] Ovsyannikov S V and Shchennikov V V 2007 *Applied Physics Letters* **90** 122103

[61] Bathula S, Jayasimhadri M, Singh N, Srivastava A K, Pulikkotil J, Dhar A and Budhani R C 2012 *Applied Physics Letters* **101** 213902

[62] Wu L, Sun Y, Zhang G-Z and Gao C-X 2014 *Materials Letters* **129** 68-71

[63] Zhao L D, Lo S H, Zhang Y, Sun H, Tan G, Uher C, Wolverton C, Dravid V P and Kanatzidis M G 2014 *Nature* **508** 373-377

[64] Ghosh A, Gusmão M S, Chaudhuri P, Michielon de Souza S, Mota C, Trichês D M and Frota H O 2016 *Computational Condensed Matter* **9** 77-81

[65] Rehman S u, Butt F K, Tariq Z, Hayat F, Gilani R and Aleem F 2017 *Journal of Alloys and Compounds* **695** 194-201

[66] Ehm L, Knorr K, Dera P, Krimmel A, Bouvier P and Mezouar M 2004 *Journal of Physics: Condensed Matter* **16** 3545-3554

[67] Shen S, Zhu W, Deng Y, Zhao H, Peng Y and Wang C 2017 *Applied Surface Science* **414** 197-204

[68] Prasad K G, Kannam S K and Sathian S P 2019 *Physica B: Condensed Matter* **556** 97-102

[69] Wang X and Liu X 2020 *Inorganic Chemistry Frontiers* **7** 2890-2908

[70] Medlin D L and Snyder G J 2009 *Current Opinion in Colloid & Interface Science* **14** 226-235

[71] Dong X, Cui W, Liu W-D, Zheng S, Gao L, Yue L, Wu Y, Wang B, Zhang Z, Chen L and Chen Z-G 2021 *Journal of Materials Science & Technology* **86** 204-209

[72] Li C, Guo D, Li K, Shao B, Chen D, Ma Y and Sun J 2018 *Physica E: Low-dimensional Systems and Nanostructures* **97** 392-400

[73] Xiao Y, Wang D, Zhang Y, Chen C, Zhang S, Wang K, Wang G, Pennycook S J, Snyder G J, Wu H and Zhao L D 2020 *J Am Chem Soc* **142** 4051-4060

[74] Zhang X W, Liu C H, Tao Y, Li Y H, Guo Y L, Chen Y F, Zeng X C and Wang J L 2020 *Advanced Functional Materials* **30** 2001200

[75] Sakane S, Ishibe T, Mizuta K, Fujita T, Kiyofuji Y, Ohe J-i, Kobayashi E and Nakamura Y 2021 *Journal of Materials Chemistry A* **9** 4851-4857

[76] Liu H-T, Sun Q, Zhong Y, Xia C-L, Chen Y, Chen Z-G and Ang R 2022 *Chemical Engineering Journal* **428** 132601

[77] Ma Z, Wang C, Chen Y, Li L, Li S, Wang J and Zhao H 2021 *Materials Today Physics* **17** 100350

[78] Pakdel A, Guo Q, Nicolosi V and Mori T 2018 *Journal of Materials Chemistry A* **6** 21341-21349

[79] Efthimiopoulos I, Berg M, Bande A, Puskar L, Ritter E, Xu W, Marcelli A, Ortolani M, Harms M, Muller J, Speziale S, Koch-Muller M, Liu Y, Zhao L D and Schade U 2019 *Phys Chem Chem Phys* **21** 8663-8678

[80] Doak J W, Michel K J and Wolverton C 2015 *Journal of Materials Chemistry C* **3** 10630-10649

[81] Zhao J, Yu Z, Hu Q, Wang Y, Schneeloch J, Li C, Zhong R, Wang Y, Liu Z and Gu G 2017 *Phys Chem Chem Phys* **19** 2207-2216

[82] Yin Z, Liu Z, Yu Y, Zhang C, Chen P, Zhao J, He P and Guo X 2021 *ACS Appl Mater Interfaces* **13** 57638-57645

[83] Lee K H, Kim S-i, Lim J-C, Cho J Y, Yang H and Kim H-S 2022 *Advanced Functional Materials* **32** 2203852

[84] Li J, Zhang X, Duan B, Cui Y, Yang H, Wang H, Li J, Hu X, Chen G and Zhai P 2019 *Journal of Materiomics* **5** 81-87

[85] Zhao K, Wang Y, Xin C, Sui Y, Wang X, Wang Y, Liu Z and Li B 2016 *Journal of Alloys and Compounds* **661** 428-434

[86] Mahmood Q, Hassan M, Ahmad S H A, Shahid A and Laref A 2018 *Journal of Physics and Chemistry of Solids* **120** 87-95

[87] Noor N A, Mahmood Q, Hassan M, Laref A and Rashid M 2018 *J Mol Graph Model* **84** 152-159

[88] Batool A, Faridi M A, Mahmood Q, Ul Haq B, Laref A and Awan S E 2018 *Journal of Physics and Chemistry of Solids* **123** 70-75

[89] Noor N A, Hassan M, Rashid M, Alay-e-Abbas S M and Laref A 2018 *Materials Research Bulletin* **97** 436-443

[90] Ning S, Huang S, Zhang Z, Zhang R, Qi N and Chen Z 2020 *Phys Chem Chem Phys* **22** 14621-14629

[91] Hu C, Ni P, Zhan L, Zhao H, He J, Tritt T M, Huang J and Sumpter B G 2018 *Rare Metals* **37** 316-325

[92] Saini A, Nag S G, Singh R and Kumar R 2020 *Journal of Alloys and Compounds* **818** 152929

[93] Gaul A, Peng Q, Singh D J, Ramanath G and Borca-Tasciuc T 2017 *Phys Chem Chem Phys* **19** 12784-12793

[94] Aliabad H A R, Rabbanifar S and Khalid M 2019 *Physica B: Condensed Matter* **570** 100-109

[95] Starý Z, Horák J, Stordeur M and Stölzer M 1988 *Journal of Physics and Chemistry of Solids* **49** 29-34

[96] Navrátil J, Starý Z and Plecháček T 1996 *Materials Research Bulletin* **31** 1559-1566

[97] Soni A, Shen Y, Yin M, Zhao Y, Yu L, Hu X, Dong Z, Khor K A, Dresselhaus M S and Xiong Q 2012 *Nano Lett* **12** 4305-4310

[98] Pan Y, Wei T-R, Wu C-F and Li J-F 2015 *Journal of Materials Chemistry C* **3** 10583-10589

[99] Hu L P, Gao H L, Liu X H, Xie H H, Shen J J, Zhu T J and Zhao X B 2012 *Journal of Materials Chemistry* **22** 16484-16490

[100] Wu H, Chang C, Feng D, Xiao Y, Zhang X, Pei Y, Zheng L, Wu D, Gong S, Chen Y, He J, Kanatzidis M G and Zhao L-D 2015 *Energy & Environmental Science* **8** 3298-3312

[101] Qian X, Wu H, Wang D, Zhang Y, Wang J, Wang G, Zheng L, Pennycook S J and Zhao L-D 2019 *Energy & Environmental Science* **12** 1969-1978

[102] Fu C, Zhu T, Liu Y, Xie H and Zhao X 2015 *Energy & Environmental Science* **8** 216-220

[103] Cui J, Li S, Xia C, Chen Y and He J 2021 *Journal of Materiomics* **7** 1190-1197

[104] Guo S-D and Wang J-L 2016 *RSC Advances* **6** 31272-31276

[105] Laukhin V, Copie O, Rozenberg M J, Weht R, Bouzehouane K, Reyren N, Jacquet E, Bibes M, Barthelemy A and Herranz G 2012 *Phys Rev Lett* **109** 226601

[106] Liu Z, Guo X, Li R, Qin J, Li H, Chen X and Zhou X 2019 *Journal of Materiomics* **5** 649-656

[107] He R, Zhu T, Wang Y, Wolff U, Jaud J-C, Sotnikov A, Potapov P, Wolf D, Ying P, Wood M, Liu Z, Feng L, Rodriguez N P, Snyder G J, Grossman J C, Nielsch K and Schierning G 2020 *Energy & Environmental Science* **13** 5165-5176

[108] Xie H, Wang H, Pei Y, Fu C, Liu X, Snyder G J, Zhao X and Zhu T 2013 *Advanced Functional Materials* **23** 5123-5130

[109] Shuai J, Mao J, Song S, Zhu Q, Sun J, Wang Y, He R, Zhou J, Chen G, Singh D J and Ren Z 2017 *Energy & Environmental Science* **10** 799-807

[110] Xia C, Cui J and Chen Y 2020 *ACS Applied Electronic Materials* **2** 2745-2749

[111] Khumtong T, Sukwisute P, Sakulkalavek A and Sakdanuphab R 2017 *Journal of Electronic Materials* **46** 3166-3171

[112] Liu Y, Zhang Y, Ortega S, Ibanez M, Lim K H, Grau-Carbonell A, Marti-Sanchez S, Ng K M, Arbiol J, Kovalenko M V, Cadavid D and Cabot A 2018 *Nano Lett* **18** 2557-2563

[113] Jiang L, Han L, Lu C, Yang S, Liu Y, Jiang H, Yan Y, Tang X and Yang D 2021 *ACS Appl Mater Interfaces* **13** 11977-11984

[114] Guo X, Qin J, Jia X, Ma H and Jia H 2017 *Journal of Alloys and Compounds* **705** 363-368

[115] Shi W, Deng T, Wu G, Hippalgaonkar K, Wang J S and Yang S W 2019 *Adv Mater* **31** e1901956

[116] Chen Z-G, Shi X, Zhao L-D and Zou J 2018 *Progress in Materials Science* **97** 283-346

[117] Bu K, Luo H, Guo S, Li M, Wang D, Dong H, Ding Y, Yang W and Lu X 2020 *J Phys Chem Lett* **11** 9702-9707

[118] Zhou Y, Meng F, He J, Benton A, Hu L, Liu F, Li J, Zhang C, Ao W and Xie H 2020 *ACS Appl Mater Interfaces* **12** 31619-31627

[119] Peng K, Wu H, Yan Y, Guo L, Wang G, Lu X and Zhou X 2017 *Journal of Materials Chemistry A* **5** 14053-14060

[120] Wang Z, Alaniz J E, Jang W, Garay J E and Dames C 2011 *Nano Lett* **11** 2206-2213

[121] Deng L, Li D N, Qin J M and Duan Q 2019 *Inorg Chem* **58** 4033-4037

[122] Liu H, Zhang X, Li S, Zhou Z, Liu Y and Zhang J 2016 *Journal of Electronic Materials* **46** 2629-2633

[123] Wu Y, Zhai R, Zhu T and Zhao X 2017 *Materials Today Physics* **2** 62-68

[124] Tang Z, Hu L, Zhu T, Liu X and Zhao X 2015 *Journal of Materials Chemistry C* **3** 10597-10603

[125] Wang L B, Ni J, Jia X P, Qin J M, Guo X and Deng L 2017 *Journal of Alloys and Compounds* **691** 452-456

[126] Suzuki A, Kitagawa H, Hirayama K, Pham A H, Morito S, Etoh T and Kikuchi K 2019 *Journal of Electronic Materials* **49** 2832-2837

[127] Sun B, Zhao J, Li Y, Cao L, Yang Y, Fan X, Liu X, Wang C, Huang X, Wang X, Sun Y and Ma H 2020 *The Journal of Physical Chemistry C* **124** 9082-9088

[128] Guo X, Qin J, Jia X and Jiang D 2018 *Inorganic Chemistry Frontiers* **5** 1540-1544

[129] Zhu T, Hu L, Zhao X and He J 2016 *Adv Sci (Weinh)* **3** 1600004

[130] Yu Y, Zhang S, Mio A M, Gault B, Sheskin A, Scheu C, Raabe D, Zu F, Wuttig M, Amouyal Y and Cojocaru-Miredin O 2018 *ACS Appl Mater Interfaces* **10** 3609-3615

[131] Imai Y, Mori Y, Nakamura S and Takarabe K-i 2016 *Journal of Alloys and Compounds* **664** 369-377

[132] Hu L, Zhu T, Liu X and Zhao X 2014 *Advanced Functional Materials* **24** 5211-5218

[133] Xie L, Chen Y J, Liu R H, Song E H, Xing T, Deng T T, Song Q F, Liu J J, Zheng R K, Gao X, Bai S Q and Chen L D 2020 *Nano Energy* **68** 104347

[134] Zhang Y, Wu L, Zhang J, Xing J and Luo J 2016 *Acta Materialia* **111** 202-209

[135] Lei C and Goda K 2018 *Nature Photonics* **12** 190-191

[136] Guo F K, Cui B, Li C, Wang Y M, Cao J, Zhang X H, Ren Z F, Cai W and Sui J H 2021 *Advanced Functional Materials* **31** 2101554

[137] Kim K T, Min T S, Kim S-D, Choi E-A, Kim D W and Choi S-Y 2019 *Nano Energy* **55** 486-493

[138] Cai B, Li J, Sun H, Zhang L, Xu B, Hu W, Yu D, He J, Zhao Z, Liu Z and Tian Y 2018 *Science China Materials* **61** 1218-1224

[139] Hu L P, Zhang Y, Wu H J, Li J Q, Li Y, Mckenna M, He J, Liu F S, Pennycook S J and Zeng X R 2018 *Advanced Energy Materials* **8** 1802116

[140] Sun H, Jia X, Deng L, Lv P, Guo X, Sun B, Zhang Y, Liu B and Ma H 2014 *Journal of Alloys and Compounds* **615** 1056-1059

[141] Liu B, Ma H, Ji G, Chen J, Liu H, Zhang Y and Jia X 2019 *Journal of Alloys and Compounds* **789** 881-886

[142] Snyder G J and Toberer E S 2008 *Nat Mater* **7** 105-114
[143] Chen Z, Zhang X and Pei Y 2018 *Adv Mater* **30** e1705617
[144] Toberer E S, Zevalkink A and Snyder G J 2011 *Journal of Materials Chemistry* **21** 15843-15852
[145] Xue L S, Fang C, Shen W X, Shen M J, Ji W T, Zhang Y W, Zhang Z F and Jia X P 2019 *Physics Letters A* **383** 125917
[146] Zhou X, Yan Y, Lu X, Zhu H, Han X, Chen G and Ren Z 2018 *Materials Today* **21** 974-988
[147] Abdellaoui L, Chen Z W, Yu Y, Luo T, Hanus R, Schwarz T, Villoro R B, Cojocaru-Miredin O, Snyder G J, Raabe D, Pei Y Z, Scheu C and Zhang S Y 2021 *Advanced Functional Materials* **31** 2101214
[148] Hu P, Wei T R, Qiu P, Cao Y, Yang J, Shi X and Chen L 2019 *ACS Appl Mater Interfaces* **11** 34046-34052
[149] Callaway J 1959 *Physical Review* **113** 1046-1051
[150] Zhu T J, Fu C G, Xie H H, Liu Y T, Feng B, Xie J and Zhao X B 2013 *EPL (Europhysics Letters)* **104** 46003
[151] Yuan K, Sun Z, Zhang X and Tang D 2019 *Sci Rep* **9** 9490
[152] Li J, Chen G, Duan B, Zhu Y, Hu X, Zhai P and Li P 2016 *Journal of Electronic Materials* **46** 2570-2575
[153] Sun B, Jia X, Huo D, Sun H, Zhang Y, Liu B, Liu H, Kong L and Ma H 2016 *Journal of Alloys and Compounds* **658** 19-22